Developmental Cognitive Neuroscience 39 (2019) 100687

Contents lists available at ScienceDirect

Developmental Cognitive Neuroscience

journal homepage: www.elsevier.com/locate/dcn

Attenuated long-range temporal correlations of electrocortical oscillations in patients with autism spectrum disorder

Huibin Jia, Dongchuan Yu*

Key Laboratory of Child Development and Learning Science of Ministry of Education, Research Center for Learning Science, School of Biological Sciences & Medical Engineering, Southeast University, Nanjing, Jiangsu, China

ARTICLE INFO

Keywords:
Long-Range temporal correlations
Autism spectrum disorder
Scale-Invariance
Electrocortical oscillations

ABSTRACT

The aim of this study was to investigate the long-range temporal correlations (LRTCs) of instantaneous amplitude of electrocortical oscillations in patients with autism spectrum disorder (ASD). Using the resting-state electroencephalography (EEG) of 15 patients with ASD (aged between 5˜18 years, mean age = 11.6 years, SD = 4.4 years) and 18 typical developing (TD) people (aged between 5˜18 years, mean age = 8.9 years, SD = 2.4 years), we estimated the LRTCs of neuronal oscillations amplitude of 84 predefined cortical regions of interest using detrended fluctuation analysis (DFA) after confirming the presence of scale invariance. We found that the DFA exponents of instantaneous amplitude of beta and low-gamma oscillations were significantly attenuated in patients with ASD compared to TD participants. Moreover, the regions with attenuated DFA exponent were mainly located in social functions related cortical networks, including the default mode network (DMN), the mirror neuron system (MNS) and the salience network (SN). These findings suggest that ASD is associated with highly volatile neuronal states of electrocortical oscillations, which may be related to social and cognitive dysfunction in patients with ASD.

1. Introduction

The autism spectrum disorder (ASD) is a range of neurodevelopmental conditions characterized by challenges with social skills, repetitive behaviors, language and nonverbal communication (Lord et al., 1994). This neuropsychiatric disorder is generally diagnosed in early childhood and brings heavy burden to the affected individuals and their caregivers (Leigh and Du, 2015). Recent advances in neuroimaging techniques provided significant insights into the neurobiological mechanisms of ASD, which revealed that ASD is closely associated with atypical functional connectivity or spatial dependency among certain regions of interest (ROIs) (Belmonte et al., 2004). Using functional magnetic resonance imaging (fMRI), altered functional connectivity between default mode network (DMN) regions, which play crucial role in mentalizing, self-reference and social cognition, is among the most commonly reported findings in people with ASD (Padmanabhan et al., 2017). Note that, most of these studies focused on the aberrant spatial organization of large-scale brain networks and few studies were involved in the temporal structure of the neuronal activities of autistic brain.

Previous studies on the temporal dependency of neuronal activities have consistently revealed that the fluctuations of neuronal signals at many levels of nervous system are governed by power-law-form long-range temporal correlations (LRTCs), which suggests that the brain could operate near a critical state and may represent an optimal compromise for the competing demands of stability and information transmission in neuronal networks (Beggs and Plenz, 2003; Hardstone et al., 2012). The LRTCs in physiological signals can be assessed through various methods, such as detrended fluctuation analysis (DFA) (Peng et al., 1995). This temporal property of brain oscillations could be modulated by several cognitive, demographic and pathologic variables, and is considered as a promising biomarker for pre-clinical studies (Hardstone et al., 2012; Linkenkaer-Hansen et al., 2005; Smit et al., 2011). Since some of the aberrant functions commonly observed in ASD (e.g., language, social cognition and communication) require sustained cognitive operations, it's necessary to explore the LRTCs of intrinsic brain activities in these patients.

Using resting-state fMRI technique, Lai et al. (2010) provided preliminary evidence that ASD is associated with significantly attenuated LRTCs in regions previously reported to be involved in autism (Lai et al., 2010). A recently study conducted by our team found that the LRTCs of hemoglobin concentration signals within left temporal region and bilateral temporo-occipital regions recorded via functional near infrared spectroscopy (fNIRS) were also attenuated in ASD patients (Jia

* Corresponding author. Current address at: Room 302, Liwenzheng Building, Southeast University, No. 2, Sipailou, Xuanwu District, Nanjing, 210096, China.
E-mail address: dcyu@seu.edu.cn (D. Yu).

https://doi.org/10.1016/j.dcn.2019.100687
Received 29 October 2018; Received in revised form 24 June 2019; Accepted 26 July 2019
Available online 30 July 2019

et al., 2018). However, building a neurophysiological model of ASD requires that specific changes within different frequencies be investigated, which could not be accomplished with fMRI or fNIRS technique.

Here, using the resting-state electroencephalogram (EEG) datasets of the Healthy Brain Network (HBN) (Alexander et al., 2017), we examined whether the LRTCs of electrocortical signals were attenuated in patients with ASD, and determined the frequency bands in which reduced LRTCs occurred. We hypothesized that there would be attenuation of LRTCs in these patients, especially within brain regions known to be involved in autism, such as the DMN.

2. Material and methods

2.1. Participants

The resting-state EEG datasets of 15 patients with ASD and 18 typical developing (TD) people from HBN were selected here. All the participants in both groups were male, aged between 5˜18 years (ASD: mean age = 11.6 years, SD = 4.4 years; TD: mean age = 8.9 years, SD = 2.4 years) and right-handed, with IQ higher than 66. For the participants in the ASD group, diagnosis was established by clinical team based on a computerized web-based version of the Schedule for Affective Disorders and Schizophrenia - Children's version (Kaufman et al., 1997) and Autism Diagnostic Observation Schedule (ADOS) (Lord et al., 2012). No diagnosis was given to the participants in the TD group. For more information about this database and its inclusion & exclusion criteria, see http://fcon_1000.projects.nitrc.org/indi/cmi_healthy_brain_network/inclusion.html.

2.2. EEG recording

Spontaneous brain activities were measured with EEG for about 5 min. In EEG collection, the participants were instructed to open or close their eyes at various time points in a sound-shielded room. In the eye-open periods, they were asked to view a fixation cross in the center of computer screen. A 128-channel Hydro-Cel Geodesic system covering the entire scalp (EGI Inc., Eugene, Oregon, USA) was used. During online recording, the EEG data were referenced to an electrode over the vertex of the head (i.e., Cz). The impedances of all electrodes were kept lower than 40 kΩ. The sampling frequency was 500 Hz with a bandpass filter of 0.1–100 Hz.

The data collection in HBN was conducted in accordance with the Declaration of Helsinki and approved by the Chesapeake Institutional Review Board. Written consent were obtained from their legal guardians and written assent obtained from the participants.

2.3. EEG data preprocessing

EEG data were preprocessed using EEGLAB (Delorme and Makeig, 2004). Firstly, the electrodes located on the neck/face were excluded from further preprocessing. Secondly, the "bad electrodes" (i.e., those electrodes with large drift longer than 1 min) were identified through visual inspection and were interpolated using a spherical spline method (Perrin et al., 1989). The mean and standard deviation of electrodes interpolated across subjects were 9.2 and 1.5, respectively. Thirdly, we scrolled through the EEG signals again. Data portions with drift could be seen on other electrodes which were not interpolated in the previous step. These data portions were deleted. The remaining segments were stitched together. This operation should not significantly influence the estimation of LRTCs, which has been proved by Chen et al. (2002). Fourthly, EEG data were re-sampled to 250 Hz and band-pass filtered between 0.5 and 80 Hz through a Hamming windowed finite impulse response (FIR) filter. The order of the FIR was chosen so that it included three cycles of the lower edge of the band considered (i.e., 1500). A notch filter was used to eliminate 60 Hz line noise. Fifthly, the independent component analysis (ICA) was applied to correct data portions contaminated by eye movements & blinks, electromyography (EMG), electrocardiography (ECG) and any non-physiological artifacts. For more information about how to selection artifact-related independent components, see Chaumon et al. (2015). Lastly, the EEG data were re-referenced to a common average reference.

2.4. Source localization

The exact low resolution brain electromagnetic tomography (eLORETA) was used to calculate the intracerebral electrical source activities from the scalp electrical potentials measured at the electrode sites (Pascual-Marqui et al., 2011). It has been proved that the eLORETA provides a weighted minimum norm inverse solution and has correct localization even in the presence of structured noise, albeit with low spatial resolution (Aoki et al., 2015). Through the LORETA software (http://www.uzh.ch/keyinst/loreta.htm), the neuronal activities in current density (A/m^2) of 6239 cortical gray matter voxels with 5 mm spatial resolution using the MNI152 template were obtained for each participant (Hata et al., 2016). Then, the time-series of current density were extracted for all cortical ROIs and six frequency bands: delta (2˜4 Hz), theta (4˜8 Hz), alpha (8˜13 Hz), beta (14˜30 Hz), low-gamma (30˜55 Hz) and high-gamma (65˜80 Hz). The cortical ROIs here were defined as the 84 Brodmann areas listed in Table 1 (Mohan et al.,

Table 1
The 84 ROIs defined in the current study. R: right hemisphere; L: left hemisphere.

ROI	Brodmann area	Abbrev.	Brain regions
1/43	1L/1R	S11	Primary somatosensory cortex1
2/44	2L/2R	S12	Primary somatosensory cortex2
3/45	3L/3R	S13	Primary somatosensory cortex3
4/46	4L/4R	M1	Primary motor cortex
5/47	5L/5R	SPS	Superior parietal sulcus
6/48	6L/6R	SMA	Supplementary motor area
7/49	7L/7R	PC	precuneus
8/50	8L/8R	Pre-SMA	Pre-supplementary motor area
9/51	9L/9R	DLPFC	Dorsolateral prefrontal cortex
10/52	10 L/10R	FPC	Fronto-parietal cortex
11/53	11 L/11R	OFC	Orbital frontal cortex
12/54	13 L/13R	Insula	Insula
13/55	17 L/17R	V1	Primary visual cortex
14/56	18 L/18R	V2	Secondary visual cortex
15/57	19 L/19R	Cuneus	Cuneus
16/58	20 L/20R	ITG	Inferior temporal gyrus
17/59	21 L/21R	MTG	Medial temporal gyrus
18/60	22 L/22R	STG	Superior temporal gyrus
19/61	23 L/23R	PCC1	Posterior cingulate cortex1
20/62	24 L/24R	dACC	Dorsal anterior cingulate cortex
21/63	25 L/25R	sgACC	Subgeneual anterior cingulate cortex
22/64	27 L/27R	PHG1	Parahippocampal gyrus1
23/65	28 L/28R	HIP1	Hippocampal area1
24/66	29 L/29R	RSC1	Retrosplenial cortex1
25/67	30 L/30R	RSC2	Retrosplenial cortex2
26/68	31 L/31R	PCC2	Posterior cingulate cortex2
27/69	32 L/32R	PrACC	Pregeneual anterior cingulate cortex
28/70	33 L/33R	rACC	Rostral anterior cingulate cortex
29/71	34 L/34R	PHG2	Parahippocampal gyrus2
30/72	35 L/35R	HIP2	Hippocampal area2
31/73	36 L/36R	PHG3	Parahippocampal gyrus3
32/74	37 L/37R	OTC	Occipital-temporal cortex
33/75	38 L/38R	TP	Temporal pole
34/76	39 L/39R	AG	Angular gyrus
35/77	40 L/40R	IPS	Intra-parietal sulcus
36/78	41 L/41R	A1	Primary auditory cortex
37/79	42 L/42R	A2	Secondary auditory cortex
38/80	43 L/43R	PCG	Postcentral gyrus
39/81	44 L/44R	OIFG	Opercular part of inferior frontal gyrus
40/82	45 L/45R	IFG	Inferior frontal gyrus
41/83	46 L/46R	MPFC	Medial prefrontal cortex
42/84	47 L/47R	VLPFC	Ventrolateral prefrontal cortex

2016). The source activities of each frequency band were extracted through Hamming windowed FIR filters. The order of the FIR was chosen so that it included three cycles of the low-frequency component of the band considered (i.e., 375 for delta, 188 for theta, 94 for alpha, 54 for beta, 25 for low-gamma and 12 for high-gamma), in order to accurately detect the oscillations while also limiting the temporal integration caused by FIR.

The frequency limits of alpha band were determined by the results of power spectra analysis conducted over each ROI and each subject using fast Fourier transformation (FFT). We found that alpha peak in power spectra could be clearly seen in the occipital regions for all subjects except three ASD patients and five TD subjects. Observing the power spectra, we found that the alpha peak was located between 9 and 11 Hz. Thus, the alpha band limit was set to be 8–13 Hz in the current study.

2.5. DFA on the instantaneous amplitude of neuronal oscillations

The LRTCs of source activities were quantified through DFA (Peng et al., 1995). As has been illustrated in Hardstone et al. (2012), the procedures of DFA for each frequency band, each cortical ROI and each participant could be summarized as follows:

1 Extract the instantaneous amplitude of neuronal oscillations through the Hilbert transform. The band-pass filtered source activities should not be directly used in DFA, since they are strongly anti-correlated. Assuming X(t) and $X_H(t)$ are the band-pass filtered source activity and its Hilbert transform at sampling time t (i.e., starting from 4 ms with step 4 ms) respectively, we could obtain the analytic signal $X_{an}(t)$ via the following equation: $X_{an}(t) = X(t) + iX_H(t)$. The instantaneous amplitude of X(t) is computed as the modulus of $X_{an}(t)$. Fig. 1 shows examples of 20 s of neuronal oscillations from ROI #43 (Primary somatosensory cortex1) filtered in the beta-frequency range (13~30 Hz) of an ASD patient (panel a) and a TD subject (panel b).
2 Compute the signal profile of instantaneous amplitude. Assuming the instantaneous amplitude of X(t) is A(t), the signal profile S(t) is calculated as the cumulative sum of A(t), i.e., $S(t) = \sum_{k=1}^{t} A(k) - \langle A \rangle$, where $\langle \bullet \rangle$ represents the time-average of a time series.
3 Define a set of window lengths and compute the average fluctuation for each window length. The whole length of signal profile S(t) was divided into 50% overlapping windows of size τ with a length between 1–15 seconds (for alpha, beta, low-gamma and high-gamma bands) or a length between 2–15 seconds (for delta and theta bands) equidistantly on a logarithmic scale. The standard deviation of each segmented signal profile with length τ was evaluated after linear detrending by least-squares fit. Then the average fluctuation for window length τ, $\langle F(\tau) \rangle$, was computed as the mean standard deviation of all segmented signal profiles with length τ.
4 Plot the average fluctuations for all window lengths on double logarithmic axes and compute the slope of the least-squares line over all window sizes. The power-law or scale-invariance behavior of underlying neuronal oscillations is characterized in terms of the linear scaling between the average fluctuations and window lengths in a double logarithmic coordinate system. This plot was named as *DFA fluctuation plot* in some literatures (Hardstone et al., 2012). The slope of the least-squares line in this graph was termed as the DFA exponent, α, which could be used to quantify the LRTCs. If $0 < \alpha < 1$, then the time series is stationary signal and can be modeled by a fractional Gaussian noise (fGn) (Hardstone et al., 2012). More specifically, $0 < \alpha < 0.5$, $\alpha \approx 0.5$ and $0.5 < \alpha < 1$ imply the time series is anti-correlated, uncorrelated random process with no LRTCs, and positive correlated respectively (Gao et al., 2017). If $1 < \alpha < 2$, the time series is non-stationary and can be modeled by a fractional Brownian noise (fBn). For the current study, the linear scaling was confirmed by both a high value of coefficient of determination (i.e., $R^2 > 0.9$ for most neuronal oscillations) of the least-squares line and stringent validation tests shown below.

2.6. Validating the presence of scale-invariance

Power law (or scale invariant) decay of the auto-covariance function will result in linear scaling in the DFA fluctuation plots (Hardstone et al., 2012). However, we have no prior knowledge as to whether the signals exhibit such scale invariance. The DFA conducted on instantaneous amplitude will provide the slope of the fluctuation plot as DFA exponent with no check as to whether the fluctuation plot is genuinely linear.

Here, a maximum likelihood based model selection technique, so called *ML-DFA*, was used to assess the validity of the assumption of linearity in DFA fluctuation plots (Botcharova et al., 2013). Briefly speaking, this technique fits these log-log plots with a set of alternative models. Then, the Akaike Information Criterion (AIC), which takes into account both the number of parameters involved and the over-fitting problem, is estimated for each model (Botcharova et al., 2015). The scale-invariance is validated only if the linear model has the lowest value of AIC, compared to other models. Only those time series that were not rejected for not being linear contributed to our results.

After the presence of scale-invariance had been evaluated, the percentage of participants for which power-law scaling was accepted was calculated for each ROI, each frequency band and each group respectively.

2.7. Statistical tests

In order to test whether the DFA exponents were significantly altered in patients with ASD, independent-samples *t*-test was conducted

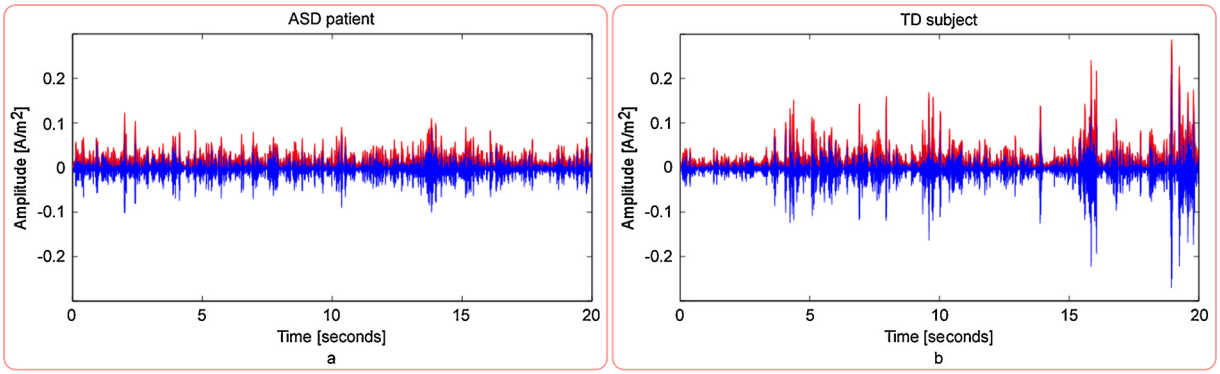

Fig. 1. Examples of 20 s neuronal oscillations from ROI #43 (Primary somatosensory cortex1) within beta band of an ASD patient (panel a) and a TD subject (panel b). Amplitude of beta oscillations is shown in blue and the amplitude envelope in red. Color should be used for this figure in print.

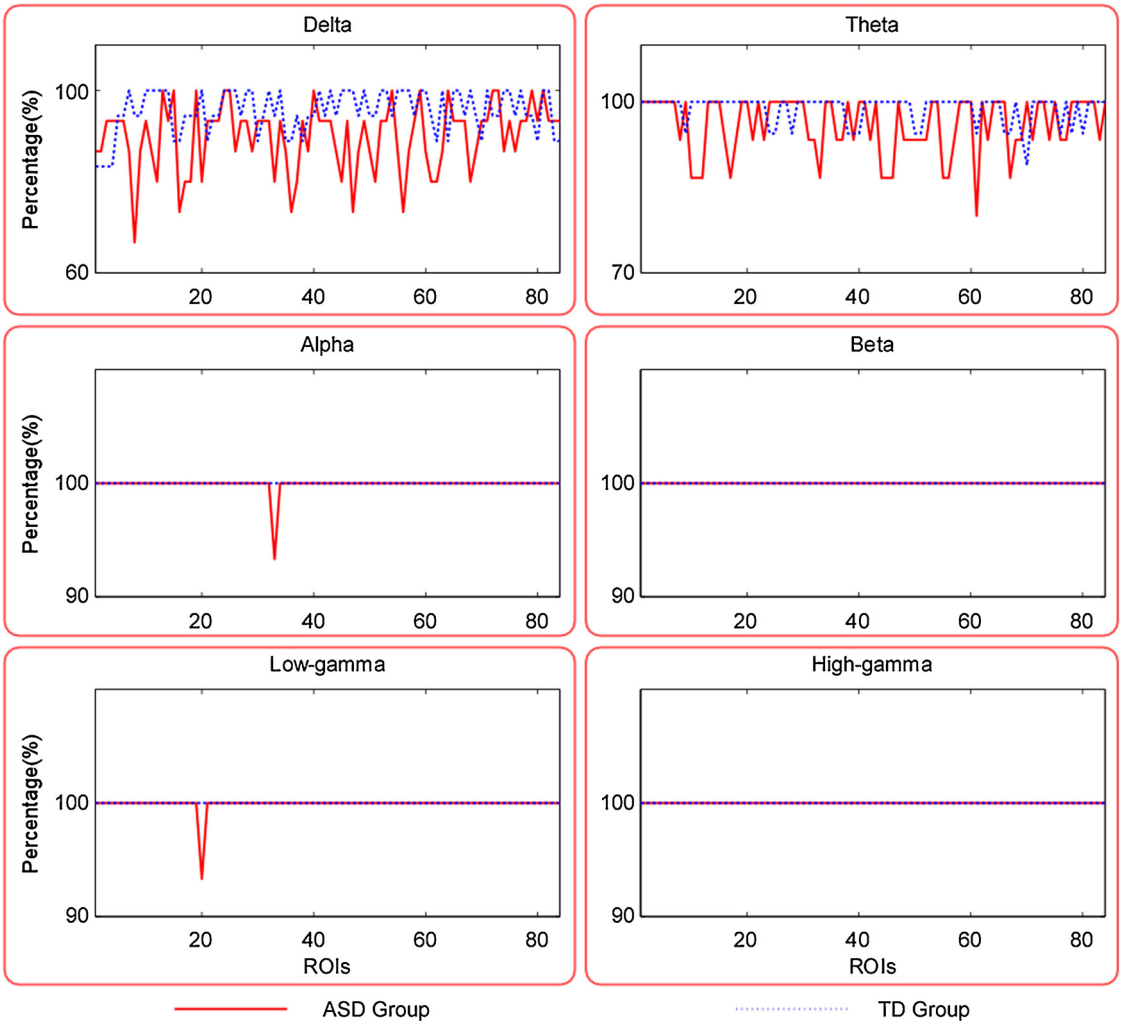

Fig. 2. The results of ML-DFA. The percentage of participants for which the presence of scale-invariance was accepted within each ROI, each group and each frequency band is presented in panel a, b, c, d, e and f. For each panel, the red solid line and the blue dashed line correspond to the ASD group and the TD group respectively. Color should be used for this figure in print.

for each ROI and each frequency band respectively. Since age may modulate the DFA exponent of brain oscillations (Smit et al., 2011), the age of each participant was included as a covariate. The statistical tests were done through the MATLAB function "gretna_GroupAnalysis" in the GRETNA software (Wang et al., 2015). In order to control multiple comparisons, the significance level (p value) was corrected using false discovery rate (FDR) procedure (Benjamini and Yekutieli, 2001). The threshold for significance was $p < 0.05$ for the statistical tests and the alpha value for FDR procedures was 0.05.

3. Results

3.1. The presence of scale-invariance

The results of ML-DFA conducted on the instantaneous amplitude of neuronal oscillations are shown in Fig. 2.

In the delta and theta bands, this percentage was relatively high, i.e., larger than 80% for most of the ROIs in both groups. When observing the higher frequency bands (i.e., alpha, beta, low-gamma and high-gamma), this percentage nearly reached 100%. Specifically, in the TD group, this percentage reached 100% for all ROIs and all the four higher frequency bands. In the ASD group, this percentage was also 100% for beta and high-gamma bands, whereas this percentage was 93.3% for alpha and low-gamma bands (i.e., the instantaneous amplitudes of source activities of one ASD patient were not found to be scale-invariant in these two bands).

3.2. The group effect on DFA exponent of instantaneous amplitude

The statistical tests showed that the DFA exponents of certain ROIs in the TD group were significantly larger than those in the ASD group for the beta band (Fig. 3) and the low-gamma band (Fig. 4). Significant results were not found in other frequency bands.

For beta band, significant group effects (TD > ASD) were found in the following cortical ROIs: 20 L (inferior temporal gyrus), 21 L (medial temporal gyrus), 22 L (superior temporal gyrus), 34 L (parahippocampal gyrus2), 38 L (temporal pole), 1R (primary somatosensory cortex1), 2R (primary somatosensory cortex2), 3R (primary somatosensory cortex3), 4R (primary motor cortex), 11R (orbital frontal cortex), 13R (insula), 38R (temporal pole), 43R (postcentral gyrus), 44R (opercular part of inferior frontal gyrus) and 47R (ventrolateral prefrontal cortex).

For low-gamma band, significant group effects (TD > ASD) were found in the following brain regions: 20 L (inferior temporal gyrus), 21 L (medial temporal gyrus), 22 L (superior temporal gyrus), 34 L (parahippocampal gyrus2), 38 L (temporal pole), 1R (primary somatosensory cortex1), 2R (primary somatosensory cortex2), 3R (primary somatosensory cortex3), 11R (orbital frontal cortex), 13R (insula), 21R

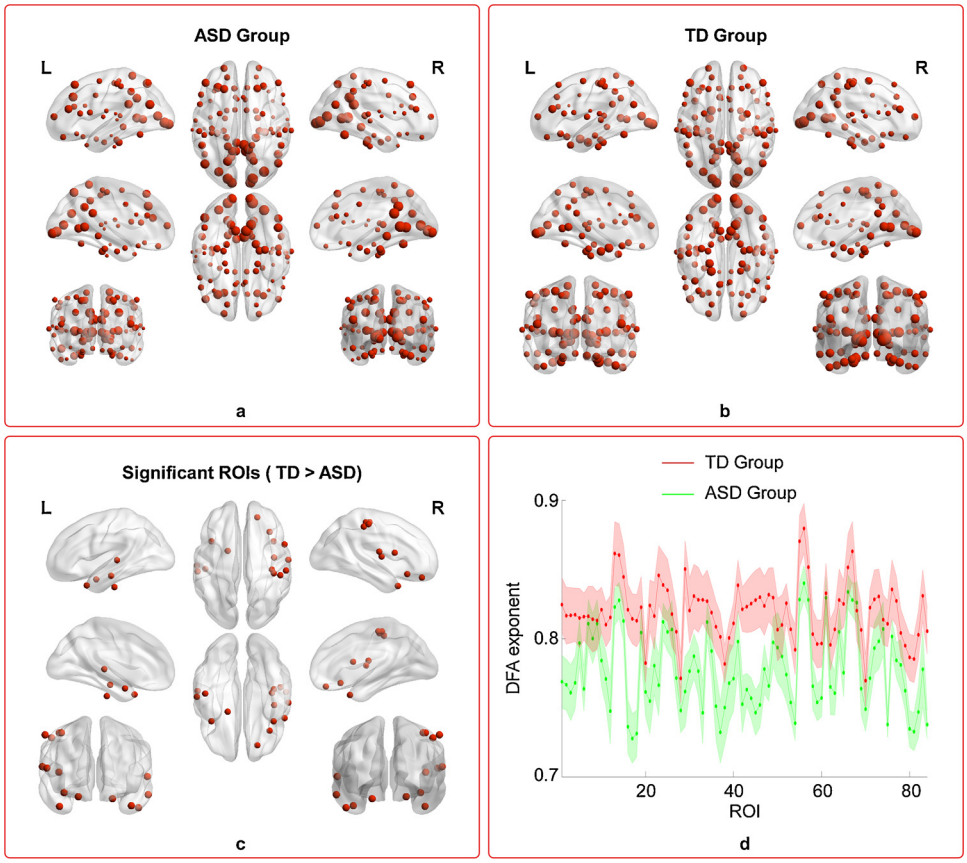

Fig. 3. The DFA exponents of instantaneous amplitude of beta oscillations. Panels a and b show the DFA exponent of each cortical ROI for ASD group and TD group, respectively. The size of each ROI corresponds to its magnitude of DFA exponent. Panel c shows the ROIs with significant group effect (TD > ASD) after FDR correction. The continuous curves and shade regions in panel d show the group-level average DFA exponents and related standard errors of all 84 ROIs for both groups, respectively (ASD group: green curve and shade region; TD group: red curve and shade region). Color should be used for this figure in print.

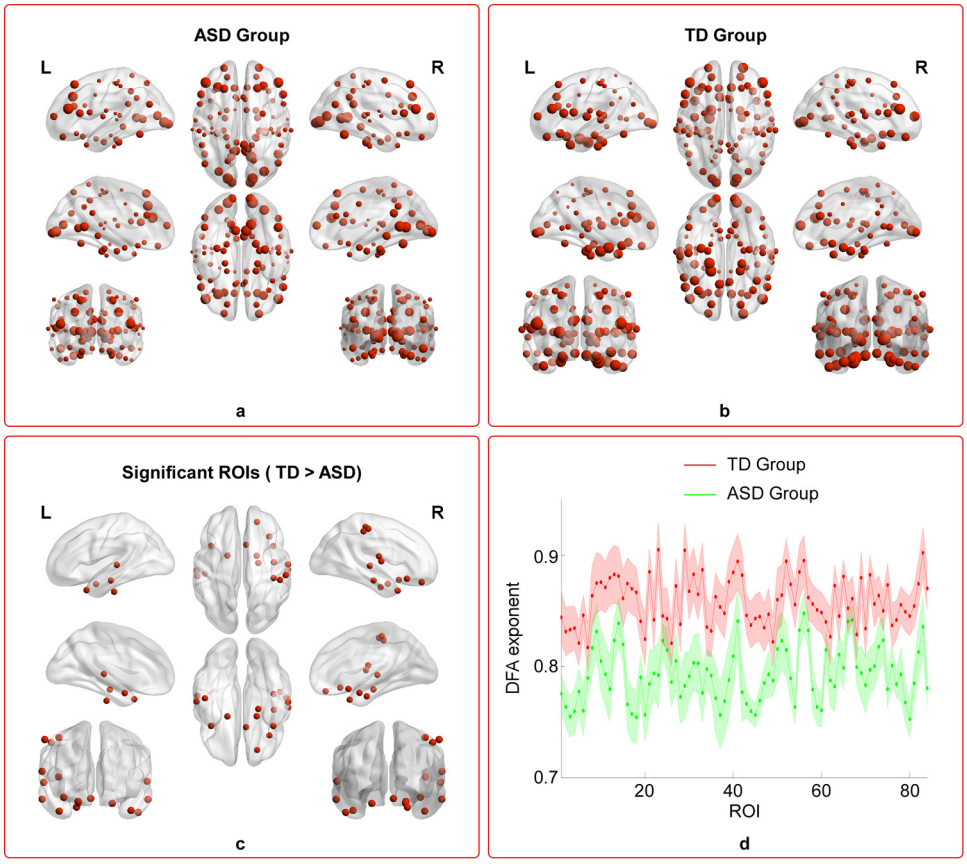

Fig. 4. The DFA exponents of instantaneous amplitude of low-gamma oscillations. Panels a and b show the DFA exponents of each cortical ROI for ASD group and TD group, respectively. The size of each ROI corresponds to its magnitude of DFA exponent. Panel c shows the cortical ROIs with significant group effect (TD > ASD) after FDR correction. The continuous curves and shade regions in panel d show the group-level average DFA exponents and related standard errors of all 84 ROIs for both groups, respectively (ASD group: green curve and shade region; TD group: red curve and shade region). Color should be used for this figure in print.

(medial temporal gyrus), 22R (superior temporal gyrus), 25R (subgeneual anterior cingulate cortex), 28R (hippocampal area), 34R (parahippocampal gyrus2), 38R (temporal pole), 43R (postcentral gyrus) and 47R (ventrolateral prefrontal cortex).

In summary, several interesting results were revealed. Firstly, compared to beta band, more ROIs with significant group effect (TD > ASD) were found for low-gamma band oscillations. Besides, more ROIs with significant group effect (TD > ASD) were revealed in the right hemisphere compared to the left hemisphere. Secondly, cortical ROIs with significantly reduced DFA exponents for both beta and low-gamma oscillations in ASD group include left inferior temporal gyrus (ITG), left medial temporal gyrus (MTG), left superior temporal gyrus (STG), left temporal pole (TP), left parahippocampal gyrus (PHG), right primary somatosensory cortex (S1), right orbital frontal cortex (OFC), right insular, right temporal pole (TP), right postcentral gyrus (PCG) and right ventrolateral prefrontal cortex (VLPFC).

4. Discussion

4.1. The scale-free dynamics and LRTCs in brain oscillations

Scale-free fluctuations and LRTCs are ubiquitous in human neural activities, which suggests that the brain may operate at, or close to, critical regime (Palva et al., 2013). It has been widely recognized that any system operating at criticality could maximize their dynamic range of information processing and communication, and should have high efficiency in transmitting information and a readiness to respond to environmental changes (Botcharova et al., 2014; Linkenkaer-Hansen et al., 2001). Here, we validated the presence of scale invariance in the instantaneous amplitude through ML-DFA (Botcharova et al., 2013). The presence of scale-invariance could be seen in most of the brain oscillations across all the ROIs, all the six frequency bands investigated and all the participants in both groups. Moreover, observing the results shown in Fig. 2, we could find two interesting results. Firstly, the percentages of TD participants for which the presence of scale-invariance was confirmed were larger than those of ASD patients for all the six frequency bands and nearly all the ROIs. This result may indicate that although scale-invariance could be detected in these patients, this scale-free property was disrupted. Secondly, it seems that these percentages were much larger in higher frequency bands, compared to those of lower frequency bands, which may be caused by the band-pass filtering before DFA.

The LRTCs are believed to be associated with model dynamical systems that show efficiency in learning, memory formation, rapid information transfer and network organization (Botcharova et al., 2014). Previous researches suggested that stronger LRTCs correspond to larger integration times of physiological processes, and LRTCs are positive correlated with the ability of brain to maintain transiently stable oscillations in support of active neuronal representations during sustained cognitive operations (Smit et al., 2011). Since some of the aberrant functions commonly observed in ASD (e.g., language, social cognition and communication) require sustained cognitive operations, it's necessary to explore the scale-free dynamics of intrinsic brain activities in patients with ASD.

4.2. The attenuated LRTCs of instantaneous amplitude of oscillatory activities in autistic brain

We found that the LRTCs of beta and low-gamma oscillations of some ROIs were attenuated in our patients, compared to those of TD subjects. These ROIs mainly involved the key nodes in the default mode network (e.g., MTG, TP, PHG and HIP), mirror neuron system (e.g., S1, PCG, M1, VLPFC and IFG) and salience network (e.g., insular and ACC) (Iacoboni and Dapretto, 2006; Padmanabhan et al., 2017; Uddin et al., 2013), which are highly relevant to the social dysfunction in ASD (Hamilton, 2013; Padmanabhan et al., 2017; Uddin et al., 2013). The DMN is a core brain system for self-referential processing (i.e., the ability to process social information relative to oneself) and mentalizing (i.e., the ability to infer the mental states of others) (Buckner et al., 2008). The mirror neuron system (MNS), which contains cells that fire not only when the human is in action but also when he/she observes others carrying out the same actions, is a key network hypothesized to play a role in many social, cognitive and language-related abilities (Chen and Yuan, 2008; Oberman et al., 2007). The salience network (SN), composed of the insular cortex and ACC, is involved in interoceptive and affective processes and the identification of relevant internal and extrapersonal stimuli to guide behavior, and is closely associated with the ability of social responsiveness through modulating the attention to social stimuli (Uddin et al., 2013). Considering the core functions of DMN, MNS and SN on social cognition, it's reasonable that attenuated LRTCs were mainly found in the ROIs of these systems.

We also tested whether the power spectra were significantly altered in our patients through independent samples t-tests with the age of each participant as a covariate, which were conducted for each ROI and each band respectively. Significant results could not be seen in all the six bands, which may suggest that there were not significant SNR or average amplitude differences between the oscillations of two groups. Previous studies revealed significantly altered power in the ASD group (Wang et al., 2013). This discrepancy may be caused by the paradigm used here (i.e., EEG recording with alternating eyes open and eyes closed periods).

The abnormal LRTCs were limited to the beta and low-gamma activities. The gamma oscillations (> 30 Hz) may be the most commonly observed oscillatory activity in ASD research (Maxwell et al., 2015). And it has been revealed that gamma activity over frontal regions could reflect DMN activity (Berkovich-Ohana et al., 2012). The gamma oscillations are thought to represent firing of inhibitory GABAergic interneurons, and a prevailing hypothesis states that loss or reduction of inhibitory interneurons may lead to impaired processing of social and emotional stimuli in ASD (Rubenstein and Merzenich, 2010). Reduced LRTCs were also found in the beta band. Previous studies revealed altered activities of beta band, which are related to the maintenance of the current sensorimotor or cognitive states in patients with ASD (Engel and Fries, 2010; Leung et al., 2014).

Smit et al. (2011) speculated that stronger LRTCs indicate stronger ability to maintain transiently stable oscillations in support of active neuronal representations during sustained cognitive operations (Smit et al., 2011). The attenuated LRTCs, expressed as decreased DFA exponent in beta and low-gamma bands, of cortical regions within social cognition related networks suggest that the impaired social abilities observed in ASD may be caused by the fact that autistic brain is associated with highly volatile, random and irregular states of neuronal oscillations.

4.3. The influence of interpolating "bad electrodes"

In the EEG preprocessing, another strategy, i.e., the bad electrodes were deleted (i.e., not interpolated), was also used. Apart from this, the EEG preprocessing steps were the same as the original manuscript. DFA was conducted on the source activities obtained via eLORETA. We found that using this strategy could not significantly affect the results, i.e., abnormal LRTCs were still limited to beta & low-gamma band, and the ROIs within DMN, MNS and SN. However, it revealed that: (1) for beta band, significant group effects were not found in the following ROIs: 34 L, 13R and 44R; (2) for low-gamma band, significant group effects were not found in the following ROIs: 34 L, 21R, and 28R.

4.4. Limitations of the current study

The limitations of this study need to be mentioned. Firstly, the EEG signals being investigated have mixed eye-open and eye-closed periods, and opening the eye or not may significantly modulate the DFA

exponent of neuronal oscillations. However, we were unable to conduct DFA on each period because of practical reasons (i.e., the length of each period was too short for DFA). Secondly, the largest window size used here is 15 s, which is shorter than many previous studies (Linkenkaer-Hansen et al., 2005). This may have resulted in the particularly high percentages of fluctuation plots being accepted as linear, and the relatively higher DFA exponents compared to those in many previous studies. After signal preprocessing, the mean length of remaining signals across subjects was 226 s and 251 s for the ASD and TD group respectively. It suggested that the maximum window size should be about 1/10th of data length (Hardstone et al., 2012). We also conducted DFA with maximum window size 20 s, and found that the results of group comparison were similar to those reported here. We did not conduct DFA with maximum window size larger than 20 s, since this may reduce the robustness of average fluctuations estimation. Since the maximum window size of some previous studies was set to be 10˜20 s (Smit et al., 2011), we believed that analyzing LRTCs with maximum window size 15 or 20 s could also provide significant insight into the neuropathological mechanism of ASD.

5. Conclusion

Here, the LRTCs of instantaneous amplitude of beta and low-gamma oscillations were attenuated in the patients with ASD. Moreover, the cortical regions with reduced LRTCs were mainly located in well-recognized brain networks associated with autism, such as the DMN, MNS and SN. These results suggest that reduced LRTCs of beta and gamma oscillations in social cognition related networks may play an important role in the dysfunction of social, communication and emotional ability commonly observed in patients with ASD.

Declaration of Competing Interest

None.

Acknowledgement

The work was supported by the National Natural Science Foundation of China under Grants 61673113, 61273224, and 61074126. It was also supported by Humanities and Social Science Fund of Ministry of Education of China under Grant 19YJC880044. No conflicts of interest, financial or otherwise, are declared by the authors.

References

Alexander, L.M., Escalera, J., Ai, L., Andreotti, C., Febre, K., Mangone, A., Vega-Potler, N., Langer, N., Alexander, A., Kovacs, M., Litke, S., O'Hagan, B., Andersen, J., Bronstein, B., Bui, A., Bushey, M., Butler, H., Castagna, V., Camacho, N., Chan, E., Citera, D., Clucas, J., Cohen, S., Dufek, S., Eaves, M., Fradera, B., Gardner, J., Grant-Villegas, N., Green, G., Gregory, C., Hart, E., Harris, S., Horton, M., Kahn, D., Kabotyanski, K., Karmel, B., Kelly, S.P., Kleinman, K., Koo, B., Kramer, E., Lennon, E., Lord, C., Mantello, G., Margolis, A., Merikangas, K.R., Milham, J., Minniti, G., Neuhaus, R., Levine, A., Osman, Y., Parra, L.C., Pugh, K.R., Racanello, A., Restrepo, A., Saltzman, T., Septimus, B., Tobe, R., Waltz, R., Williams, A., Yeo, A., Castellanos, F.X., Klein, A., Paus, T., Leventhal, B.L., Craddock, R.C., Koplewicz, H.S., Milham, M.P., 2017. An open resource for transdiagnostic research in pediatric mental health and learning disorders. Sci. Data 4 (2017), 170181.

Aoki, Y., Ishii, R., Pascual-Marqui, R.D., Canuet, L., Ikeda, S., Hata, M., Imajo, K., Matsuzaki, H., Musha, T., Asada, T., Iwase, M., Takeda, M., 2015. Detection of EEG-resting state independent networks by eLORETA-ICA method. Front. Hum. Neurosci. 9, 31.

Beggs, J.M., Plenz, D., 2003. Neuronal avalanches in neocortical circuits. J. Neurosci. 23 (35), 11167–11177.

Belmonte, M.K., Allen, G., Beckelmitchener, A., Boulanger, L.M., Carper, R.A., Webb, S.J., 2004. Autism and abnormal development of brain connectivity. J. Neurosci. 24, 9228–9231.

Benjamini, Y., Yekutieli, D., 2001. The control of the false discovery rate in multiple testing under dependency. Ann. Stat. 29 (4), 1165–1188.

Berkovich-Ohana, A., Glicksohn, J., Goldstein, A., 2012. Mindfulness-induced changes in gamma band activity - implications for the default mode network, self-reference and attention. Clin. Neurophysiol. 123, 700–710.

Botcharova, M., Berthouze, L., Brookes, M.J., Barnes, G.R., Farmer, S.F., 2015. Resting state MEG oscillations show long-range temporal correlations of phase synchrony that break down during finger movement. Front. Physiol. 6, 183.

Botcharova, M., Farmer, S.F., Berthouze, L., 2013. A maximum likelihood based technique for validating detrended fluctuation analysis (ML-DFA). arXiv 1306 (5075).

Botcharova, M., Farmer, S.F., Berthouze, L., 2014. Markers of criticality in phase synchronization. Front. Syst. Neurosci. 8 (8), 176.

Buckner, R.L., Andrewshanna, J.R., Schacter, D.L., 2008. The brain's default network: anatomy, function, and relevance to disease. Ann. N. Y. Acad. Sci. 1124 (1), 1–38.

Chaumon, M., Bishop, D.V.M., Busch, N.A., 2015. A practical guide to the selection of independent components of the electroencephalogram for artifact correction. J. Neurosci. Methods 250 (1), 47–63.

Chen, W., Yuan, T.F., 2008. Mirror neuron system as the joint from action to language. Neurosci. Bull. 24 (4), 259–264.

Chen, Z., Ivanov, P.C., Hu, K., Stanley, H.E., 2002. Effect of nonstationarities on detrended fluctuation analysis. Phys. Rev. E Stat. Nonlin. Soft Matter Phys. 65, 041107.

Delorme, A., Makeig, S., 2004. EEGLAB: an open source toolbox for analysis of single-trial EEG dynamics including independent component analysis. J. Neurosci. Methods 134 (1), 9–21.

Engel, A.K., Fries, P., 2010. Beta-band oscillations-signalling the status quo? Curr. Opin. Neurobiol. 20, 156–165.

Gao, F., Wu, X., Feng, Y., Jia, H., 2017. Attenuation of temporal correlations of neuronal oscillations in patients with mild spastic diplegia. Sci. Rep. 7 (8), 14966.

Hamilton, A.F., 2013. Reflecting on the mirror neuron system in autism: a systematic review of current theories. Dev. Cogn. Neurosci. 3 (1), 91–105.

Hardstone, R., Poil, S.S., Schiavone, G., Jansen, R., Nikulin, V.V., Mansvelder, H.D., Linkenkaer-Hansen, K., 2012. Detrended fuctuation analysis: a scale-free view on neuronal oscillations. Front. Physiol. 3, 450.

Hata, M., Kazui, H., Tanaka, T., Ishii, R., Canuet, L., Pascual-Marqui, R.D., Aoki, Y., Ikeda, S., Kanemoto, H., Yoshiyama, K., Iwase, M., Takeda, M., 2016. Functional connectivity assessed by resting state EEG correlates with cognitive decline of Alzheimer's disease – an eLORETA study. Clin. Neurophysiol. 127 (2), 1269–1278.

Iacoboni, M., Dapretto, M., 2006. The mirror neuron system and the consequences of its dysfunction. Nat. Rev. Neurosci. 7 (12), 942–951.

Jia, H., Li, Y., Yu, D., 2018. Attenuation of long-range temporal correlations of neuronal oscillations in young children with autism spectrum disorder. Neuroimage Clin. 20, 424–432.

Kaufman, J., Birmaher, B., Brent, D., Rao, U., Flynn, C., Moreci, P., Williamson, D., Ryan, N., 1997. Schedule for Affective Disorders and Schizophrenia for School-Age Children-Present and Lifetime version (K-SADS-PL): initial reliability and validity data. J. Am. Acad. Child Adolesc. Psychiatry 36 (7), 980–988.

Lai, M.C., Lombardo, M.V., Chakrabarti, B., Sadek, S.A., Pasco, G., Wheelwright, S.J., Bullmore, E.T., Baroncohen, S., Suckling, J., 2010. A shift to randomness of brain oscillations in people with autism. Biol. Psychiatry 68 (12), 1092–1099.

Leigh, J.P., Du, J., 2015. Brief report: forecasting the economic burden of autism in 2015 and 2025 in the United States. J. Autism Dev. Disord. 45 (12), 4135–4139.

Leung, R.C., Ye, A.X., Wong, S.M., Taylor, M.J., Doesburg, S.M., 2014. Reduced beta connectivity during emotional face processing in adolescents with autism. Mol. Autism 5, 51.

Linkenkaer-Hansen, K., Monto, S., Rytsälä, H., Suominen, K., Isometsä, E., Kähkönen, S., 2005. Breakdown of long-range temporal correlations in theta oscillations in patients with major depressive disorder. J. Neurosci. 25 (44), 10131–10137.

Linkenkaer-Hansen, K., Nikouline, V.V., Palva, J.M., Ilmoniemi, R.J., 2001. Long-range temporal correlations and scaling behavior in human brain oscillations. J. Neurosci. 21 (4), 1370–1377.

Lord, C., Rutter, M., DiLavore, P.C., Risi, S., Gotham, K., Bishop, S., 2012. Autism Diagnostic Observation Schedule, second edition. ADOS-2). Western Psychological Corporation, Torrence, CA.

Lord, C., Rutter, M., Le Couteur, A., 1994. Autism Diagnostic Interview-Revised: a revised version of a diagnostic interview for caregivers of individuals with possible pervasive developmental disorders. J. Autism Dev. Disord. 24 (5), 659–685.

Maxwell, C.R., Villalobos, M.E., Schultz, R.T., Herpertz-Dahlmann, B., Konrad, K., Kohls, G., 2015. Atypical laterality of resting gamma oscillations in autism Spectrum disorders. J. Autism Dev. Disord. 45 (2), 292–297.

Mohan, A., De Ridder, D., Vanneste, S., 2016. Emerging hubs in phantom perception connectomics. Neuroimage Clin. 11, 181–194.

Oberman, L.M., Pineda, J.A., Ramachandran, V.S., 2007. The human mirror neuron system: a link between action observation and social skills. Soc. Cogn. Affect. Neurosci. 2 (1), 62–66.

Padmanabhan, A., Lynch, C.J., Schaer, M., Menon, V., 2017. The Default Mode Network in Autism. Biol. Psychiatry Cogn. Neurosci. Neuroimaging 2 (6), 476–486.

Palva, J.M., Zhigalov, A., Hirvonen, J., Korhonen, O., Linkenkaer-Hansen, K., Palva, S., 2013. Neuronal long-range temporal correlations and avalanche dynamics are correlated with behavioral scaling laws. Proc. Natl. Acad. Sci. U.S.A. 110 (9), 3585–3590.

Pascual-Marqui, R.D., Lehmann, D., Koukkou, M., Kochi, K., Anderer, P., Saletu, B., Tanaka, H., Hirata, K., John, E.R., Prichep, L., 2011. Assessing interactions in the brain with exact low-resolution electromagnetic tomography. Philos. Trans. A Math. Phys. Eng. Sci. 369 (1952), 3768–3784.

Peng, C.K., Havlin, S., Stanley, H.E., Goldberger, A.L., 1995. Quantification of scaling exponents and crossover phenomena in nonstationary heartbeat time series. Chaos 5 (1), 82–87.

Perrin, F., Pernier, J., Bertrand, O., Echallier, J.F., 1989. Spherical splines for scalp potential and current density mapping. Electroencephalogr. Clin. Neurophysiol. 72 (2), 184–187.

Rubenstein, J.L.R., Merzenich, M.M., 2010. Model of autism: increased ratio of excitation/inhibition in key neural systems. Genes Brain Behav. 2 (5), 255–267.

Smit, D.J.A., De Geus, E.J.C., Van De Nieuwenhuijzen, M.E., Van Beijsterveldt, C.E.M., Van Baal, G.C.M., Mansvelder, H.D., Boomsma, D.I., Linkenkaer-Hansen, K., 2011. Scale-free modulation of resting-state neuronal oscillations reflects prolonged brain maturation in humans. J. Neurosci. 31 (37), 13128–13136.

Uddin, L.Q., Supekar, K., Lynch, C.J., Khouzam, A., Phillips, J., Feinstein, C., Ryali, S., Menon, V., 2013. Salience network-based classification and prediction of symptom severity in children with autism. JAMA Psychiat. 70 (8), 869–879.

Wang, J., Barstein, J., Ethridge, L.E., Mosconi, M.W., Takarae, Y., Sweeney, J.A., 2013. Resting state EEG abnormalities in autism spectrum disorders. J. Neurodev. Disord. 5, 24.

Wang, J., Wang, X., Xia, M., Liao, X., Evans, A., He, Y., 2015. GRETNA: a graph theoretical network analysis toolbox for imaging connectomics. Front. Hum. Neurosci. 9, 386.